Degradation Effects in Metal-Sulfur Batteries

Raphael Richter,[*,†,‡] Joachim Häcker,[†] Zhirong Zhao-Karger,[¶] Timo Danner,[†,‡] Norbert Wagner,[†] Maximilian Fichtner,[‡,¶] K. Andreas Friedrich,[†,§] and Arnulf Latz[†,‡,‖]

†*Institute of Engineering Thermodynamics, German Aerospace Center (DLR), Pfaffenwaldring 38-40, 70569 Stuttgart, Germany*
‡*Helmholtz Institute Ulm (HIU), Helmholtzstrasse 11, 89081 Ulm, Germany*
¶*Institute of Nanotechnology, Karlsruhe Institute of Technology (KIT), P.O. Box 3640, 76021 Karlsruhe, Germany*
§*Institute of Energy Storage, University of Stuttgart, Pfaffenwaldring 31, 70569 Stuttgart, Germany*
‖*Institute of Electrochemistry, University of Ulm, Albert-Einstein-Allee 47, 89081 Ulm, Germany*

E-mail: raphael.richter@dlr.de

Abstract

Metal-sulfur batteries (Me-S) are one of the most promising battery technologies and might even outperform future Li-ion batteries. However, these systems generally still show a relatively fast capacity loss, low power density, and fast self-discharge. Furthermore, the underlying mechanisms are insufficiently understood, making it difficult to systematically improve cell performance. In the present study we use a pseudo-2D continuum model to analyse the degradation behavior during cycling of Li-S and Mg-S batteries. The simulations reproduce charge and discharge curves of both systems and allow detailed investigations on the influence of material properties on degradation mechanisms. Special attention is paid to the redistribution of active sulfur during cycling and its effect on long-term stability. Finally, we demonstrate the application of the model for qualitative predictions of battery performance and lifetime of cathode designs with improved sulfur loading.

Keywords

metal-sulfur, continuum modeling, polysulfide-shuttle, degradation

1 Introduction

Li-ion batteries are approaching their theoretical limits and in the long run only moderate improvements, especially with regard to energy density, are expected. Therefore, research is focusing on future technologies. Lithium-sulfur batteries (Li-S) have been discussed for a long time as a potential next generation battery system.[1,2] In contrast to Li-ion batteries, they offer advantages in numerous aspects. Typically, lithium metal is used at the negative electrode which promises a very high energy density. At the positive electrode, reduction of sulfur provides a very high theoretical capacity. In combination, Li-S cells provide a theoretical energy density of 2800 Wh l^{-1} and 2500 Wh kg^{-1}.[3] Moreover, sulfur is abundant and non-toxic and, thus, provides a very sustainable alternative to state-of-the-art positive electrode materials in Li-Ion batteries. However, there are still chal-

lenges which need to be overcome in order to enable large scale commercialization.

Repeated plating and stripping of lithium leads to the growth of dendrites, which can cause short circuits and battery failure.[4,5] Magnesium is discussed as alternative anode material since the deposition of magnesium shows a lower tendency for dendrite formation.[6,7] Additionally, magnesium is also interesting because it is considerably more abundant than lithium. This is an important aspect taking into account the expected increase in battery production due to electric vehicles. In combination with sulfur, magnesium-sulfur batteries (Mg-S) offer a very high theoretical energy density of 3200 Wh l^{-1}[3] which makes them interesting candiates for automotive application.

However, in both systems the positive sulfur electrodes cause problems, especially with regard to dissolution and deposition of solid sulfur during operation.[8] Dissolved polysulfides are able to diffuse to the anode in a process called polysulfide shuttle.[9] On the metal surface side reactions occur which reduce the coulombic efficiency and lifetime of the battery. Reduction products passivate the surface of the negative electrode and simultaneously decrease the available sulfur at the positive electrode.[10–13]

Aditionally, the successful concept of a protective SEI, as known from Li-S batteries, or lithium batteries in general,[10–13] does not seem to be easily transferable to Mg-S cells.[14,15] Recently, novel electrolyte and cathode concepts we are able to improve the discharge capacity and cycle life significantly, demonstrating the potential of the technology.[14–18] Despite the progress, novel theoretical and analytical tools need to be developed in order to gain mechanistic understanding of the limiting processes in Mg-S batteries.

Therefore, we developed a novel continuum framework for the simulation of metal-sulfur (Me-S) batteries. The models couple the complex chemistry in Li-S and Mg-S batteries with transport of dissolved species in the electrolyte and microstructural properties of the electrodes and separator. In particular, this approach allows simulation of the polysulfide shuttle. Similar model designs for the simulation of Li-S batteries are presented in the literature,[19,20] however, have not been applied for degradation studies. Moreoever, to the best of our knowledge there is no continuum model for charge and discharge of Mg-S batteries published in the literature.

In our previous work we applied this framework to study self-discharge in metal-sulfur batteries.[21] The simulations werenused to analyze our electrochemical measurements on structurally similar Li-S and Mg-S batteries. Based on an intensive parameter study we identified fast side reactions of dissolved sulfur species at the anode as source for the fast self-discharge of Mg-S batteries. Moreover, by fitting our model to the experimental data we were able to determine kinetic parameters of polysulfide red-ox reactions on the Li and Mg metal surface, respectively.

In this work we extend our approach and give a detailed analysis of the degradation during cycling of Li-S and Mg-S cells in the same setup. A detailed description of the cells and electrochemical characterization is given in Section 2.1. Additionally, a brief summary of the modeling framework is provided in Section 2. Results of the simulations and analysis of the experiments is presented in Section 3.1. The simulations provide mechanistic understanding on the impact of sulfur redistribution as well as initial sulfur loading. These are important aspects for future commercialization of the technology. Our results aim to further extend the insights regarding the differences and similarities between Li-S and Mg-S batteries to guide the research and development of these promising battery concepts.

2 Methods

In this work we use the same setup for our measurements and simulations like in our previous publication on the self-discharge of Me-S batteries. Therefore, a detailed description of the experiments and simulation framework can be found in Ref.[21] In this work we limit the discussion to a brief overview of experimental procedures and relevant model features.

2.1 Experiment

Electrode preparation The positive composite electrodes consisting of sulfur (99.5 %, Alfa Aesar) and Ketjenblack EC-600 JD (Akzo Nobel) are prepared by the widely used melt infiltration method. The resulting powder is mixed with polyvinylidene fluoride (PVDF, Solvay Solef 5130) binder and it then coated in a solution based process (DMSO, VWR ProLab Chemicals) on a carbon-coated aluminum foil. Electrode composition after drying is determined by thermo gravimetric analysis to 48 wt.% sulfur, 42 wt.% carbon and 10 wt.% PVDF. This corresponds to a sulfur loading of approximately 0.75 mg cm^{-2}.
The negative electrode consists of a lithium metal (99.9 %, 750 µm, Alfa Aesar) or magnesium metal foil (99.9 %, 250 µm, Goodfellow), respectively. The magnesium foil is mechanically scraped prior to cell assembly to remove the oxide layer on the surface. The lithium foil is used as received.

Cell assembly Li-S and Mg-S cells are prepared in the same setup utilizing the same positive electrode and separator to avoid deviations in cell geometry between both systems. Moreover, we use in both systems the same solvent system consisting of a mixture of 1:1 vol. TEGDME (>99 %, Sigma-Aldrich) and DEGDME (anhydrous, 99.5 %, Sigma-Aldrich) without any additives.
The electrolyte for the Li-S cells contains 1 M LiTFSI (99.95 %, Sigma-Aldrich). For Mg-S cells 1.4 M $Mg(HMDS)_2$-$AlCl_3$ was prepared according to literature[3] in the above-mentioned solvent systems.
Finally, cells are assembled in Swagelok-type setup with a diameter of 22 mm. Positive and negative electrodes have a diameter of 18mm. Between both electrodes we use a layer of glass fiber separator (thickness 260 µm, 1.2 µm particle retention, Whatman) and add an electrolyte volume of 150 µL.

Electrochemical measurements For the degradation tests we use a galvanostatic cycling protocol at constant C/10 rate (167.2 mA g_S^{-1})) with a short rest time (1 h) at open cell voltage (OCV) right after cell assembly.
Li-S cells are cycled between 1.7 and 2.6 V during discharge and charge, respectively. A short constant voltage step (CV) of 5 minuntes (or < 10 % current rate) is applied at the end of the constant current (CC) charging step. Mg-S cells in contrast are cycled between 0.05 and 2.6 V with an elongated CV step at 2.6 V (8 h or < 10 % current rate).

2.2 Simulation

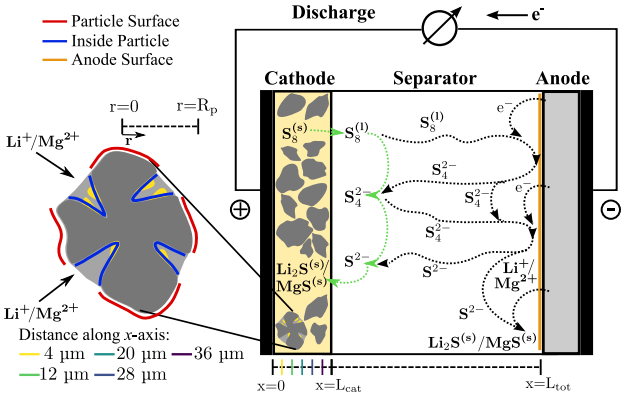

Figure 1: Schematic of a metal-sulfur cell where sulfur is infiltrated into the porous carbon structure. The coordinates of the macroscopic modeling domain (cell) and of the microscopic particle are denoted by x and r, respectively. Furthermore, the reaction mechanism at the cathode, the polysulfide shuttle, and the loss of active material due to side reactions at the anode are indicated schematically. In addition, points on the x-axis are shown for which species concentrations are shown later.

Simulation domain Fig. 1 gives a schematic overview of the cell geometry. As indicated by the magnification of the carbon particle, the multi-scale modeling domain includes both a cell and a particle scale which are coupled in our simulations. This approach allows us to model the effects of a bimodal pore size distribution. Namely, macropores between the carbon particles and micropores within particles. This is important, because the pores on particle scale contain the infiltrated sulfur.
The active surface within the particles is schematically represented by the blue lines in Fig. 1 and corresponding concentrations and

volume fractions in the particles and close to this surface are referred to as 'inside particle' in the discussion. On the other hand the surface on the particles which is in contact with the macropores is indicated by the red color in the schematic image shown in Fig. 1.

The so-called cell model represents the entire thickness of the cell from cathode to anode (x-axis). The cathode has a thickness L_{cat}= 40 µm and consists of infiltrated carbon particles (16.3 vol-%) and binder (2.3 vol-%). We assume that the pore space (81.4 vol-%) between particles is totally filled with electrolyte. The color legend along the x-axis in the cathode region shows the spacing and distribution of our control volumes, which we will refer to when showing concentrations and volume fractions. The separator between x=L_{cat} and x=L_{tot} has a porosity of 80 vol-% and is also soaked with electrolyte. The metal anode at x=L_{tot} is modeled as a flat electrode which has some surface roughness[22] not resolved in our simulations.

The so-called particle model represents the processes within the porous carbon particles. This model describes the concentrations and volume fractions that are inside the particles and are indicated by the blue region. In order to reduce computational complexity we assume representative spherical particles with a radius of 340 nm. The particles consist of a carbon matrix with 79.1 vol-% porosity or 20.9 vol-% solid volume fraction, respectively. During material preparation (cf. Sec. 2.1) the pore network is infiltrated with 20 vol-% sulfur and we assume that the remaining pore space is filled with liquid electrolyte (59.1 vol-%).

An overview of all structural parameters can be found in Table S2.

Model description A detailed derivation of model equations is presented in our previous publication. Table S1 provides an overview of the governing equations and at this point we summarize the key features of the model.

Within the simulation domain transport of all dissolved species is described using porous electrode theory for dilute electrolytes (Eqs. 1 - 9). This gives access to the temporal and spatial evolution of concentrations and electrolyte potential in the pore space of the cathode, separator, and in front of the anode surface.

In our model we use a set of representative electrolyte species which participate in a reduced set of chemical and electrochemical reactions at cathode and anode (Eqs. 13 - 17), respectively. Note, that the species in our reaction mechanism were also found in corresponding in-operando studies and we are able to qualitatively reproduce experimental charge and discharge curves.[23,24] A detailed discussion of the reaction mechanism is provided in SI section 1. At this point it is important to mention that although our simulations show a semi-quantitative agreement to experiments they are to be interpreted only qualitatively. The dissolved species in the electrolyte have to be interpreted as representative species and their concentration is the sum of several species in the electrolyte which are not considered in our reaction mechanism. Therefore, corresponding concentrations are higher than polysulfide concentrations reported in the literature.[3,23,25,26]

Additionally, we follow the dissolution and precipitation of solid sulfur as well as Li_2S and MgS, respectively. The distribution of these solids is characterized by their volume fraction (Eq. 18) and we use empirical correlations in order to include their effect on transport (Eq. 4) and active surface areas (Eqs. 11 and 19). We assume in our electrolyte a very high solubility for intermediate species e. g. MgS_4, neglecting precipitation of this phase which has also not been reported in the literature.[3,23,25,26] However, there have been indications that other species besides MgS could precipitate along the reaction chain. Since, this is still part of the current discussion, we have not considered it in the study shown here. In Sec. 8 of the supporting information we show briefly what influence a precipitation of a species along the reaction chain could have.

The electrostatic potential in the cathode is calculated using a charge balance for electrons in the carbon matrix (Eq. 20). Charge transport in the anode is not resolved and we use a constant electrode potential due to the orders of magnitude higher electrical conductivity of Li and Mg metal.

As described in the previous paragraph our multi-scale approach couples transport within particles and on cell level using the same transport theory in the electrolyte on both scales. Thereby, we are able to follow the redistribution of sulfur species from cathode particles, through the separator, to the anode surface. This intrinsically provides a description of the polysulfide shuttle.[22] Inclusion of side reactions on the anode surface (see Fig. 1) reduces the coulombic efficiency and battery capacity. Close to the anode surface we also calculate the volume fraction of solid discharge products. Their passivating effect is discussed in Sec. 3.1.2.
The governing equations summarized in Table S2 are implemented and solved in Matlab on a standard desktop computer. Using the discretization given in Table S1 the simulation time for 10 consecutive charge/discharge cycles is around 2-4 hours but strongly depends on the choice of parameters.

Parameters Table S3 summarizes transport, kinetic and thermodynamic parameters. The list of parameters is considerable and, where applicable, we use data from the literature in order to reduce the number of unknowns determined by fitting experimental data.
Transport parameters of the sulfur species are taken from the work of Kumaresan *et al.*[27] and diffusion coefficients of the Li and Mg salts are chosen to reproduce conductivity data in the literature.[28–31]
Parameters for side reactions at the anode are adopted from our previous work[21] with minor adjustments. Note, that the adjustments merely improve model predictions of the capacity fade and do not qualitatively change results of our previous publication (cf. Fig. S2).
In this work we focus the model calibration on kinetic and thermodynamic parameters of chemical and electrochemical reactions at the cathode such that the simulated charge and discharge curves reproduce the experimental data.
The corresponding sources of all model parameters are also given in Table S3.

3 Results

In this section we compare simulation results of Li-S and Mg-S batteries with the corresponding experimental data. First, we use charge and discharge simulations to interpret our measurements and to analyze battery degradation. With the help of our simulations we postulate the major processes causing capacity fade and identify differences between the two systems. Furthermore, we investigate the effect of elevated sulfur loading which demonstrates application of the model for the development of new materials and electrode formulations.

3.1 Initial cycle

The simulations use the electrochemical characterization procedures described in section 2.1. Results of the simulations and experiments in the initial cycle are presented seperately for Li-S and Mg-S cells in the paragraphs below.

3.1.1 Li-S cell

Electrochemical characterization Fig. 2 a) compares simulated (lines) and measured (symbols) charge and discharge curves in the initial cycle. In general we can report good qualitative agreement between measurements and simulations. During discharge the transition between the first and second plateau is poorly represented in our simulations. This is due to the reduced reaction mechanism which neglects intermediate discharge products. Additional reaction steps will lead to a smoother transition,[32] however, increases computational complexity. The small dip at the beginning of the second plateau is due to the nucleation of Li_2S and subsequent precipitation.
Both the experiments and the simulations show two voltage plateaus during battery charge. Despite our reduced reaction mechanism the simulations very well reproduce the transition between the plateaus.

Concentration and phase distribution Fig. 3 a) and b) show the average concentration of dissolved species and volume fractions

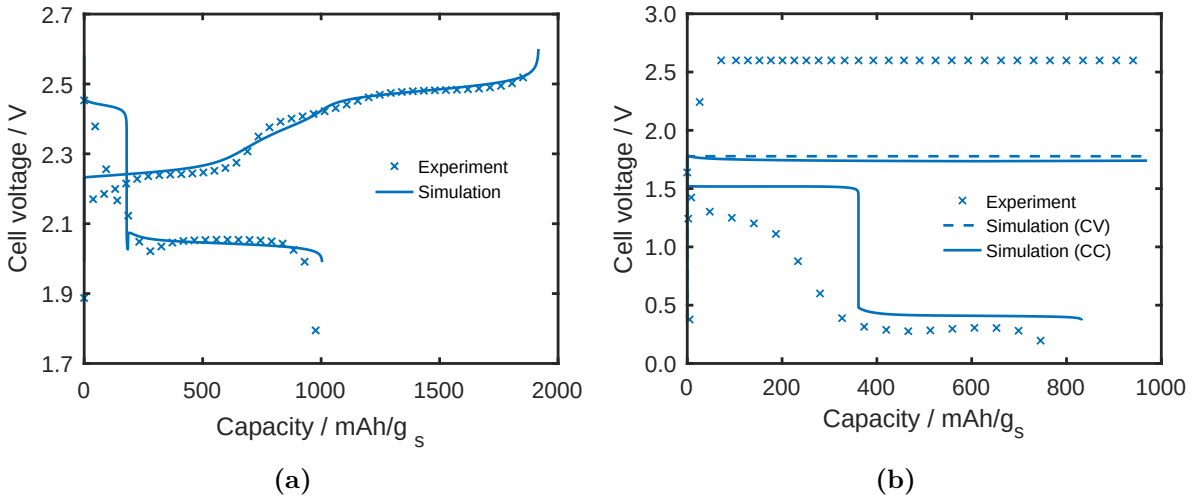

Figure 2: Charge and discharge curves of a) Li-S and b) Mg-S batteries in the 1st cycle at C/10 rate. Simulations and experiments are represented by lines and crosses, respectively.

of solid phases during the first cycle. The distance along the x-axis is given from the cathode current collector to the separator by the color code introduced in Fig. 1 of the different lines. Generally, we see minor gradients in species concentrations between particle and cell scale due to the rather low current density. Therefore, we provide only average concentrations in the cathode and at the anode surface. Additional concentration distributions highlighting concentration differences between particle and cell level can be found in Fig. S4.

The temporal evolution of species concentrations in Fig. 3 a) are key to understand the processes taking place during discharge and charge, as well as the resulting features in the cell voltage. During the upper plateau of the discharge curve, dissolved $S_8^{(l)}$ is reduced, which increases the concentration of S_4^{2-}. At the same time the concentration of dissolved $S_8^{(l)}$ remains nearly constant at about 19 mol/m^3, which corresponds to the assumed solubility limit of $S_8^{(s)}$. Due to the dissolution of sulfur clusters, the sulfur surface area and, thus, the dissolution rate decreases. At around 2 hours reduction of dissolved $S_8^{(l)}$ is not sufficient to supply the applied current density. After this point S_4^{2-} is reduced to S^{2-} which can be recognized by the short increase in S^{2-} concentration. At the same time this leads to a drop of the potential to the lower plateau.

Already shortly after the beginning of the reduction to S^{2-} the concentration drops again due to the precipitation of Li_2S. The drop in concentration also causes an increase in potential, which results in the well-known feature in the cell voltage sometimes referred to as nucleation dip.

As mentioned above concentration gradients in the electrolyte are minor and anode concentrations generally follow the concentrations in the cathode. Only the S^{2-} concentration is slightly higher at the anode. This is caused by the side reactions of polysulfides at the metal surface. This effect favors a continuous, although very slow growth of solid Li_2S at the anode. Note, that we also observe an increased precipitation of Li_2S in the particles compared to precipitation on the particle surface despite rather similar concentrations (cf. Fig. S4). This interesting behavior is described in detail in Sec. 3.4.

During charging of the cell, the processes described above take place in reverse order. Due to the polysulfide shuttle and the corresponding reduction of polysulfides on the lithium surface, the charge process takes longer than discharge at the same C-rate. This effect reduces the coulombic efficiency of the cells. However, at the end of the charge process most of the solid sulfur can be found within cathode particles. Only Li_2S which precipitates at the anode can not be dissolved again and causes an irreversible

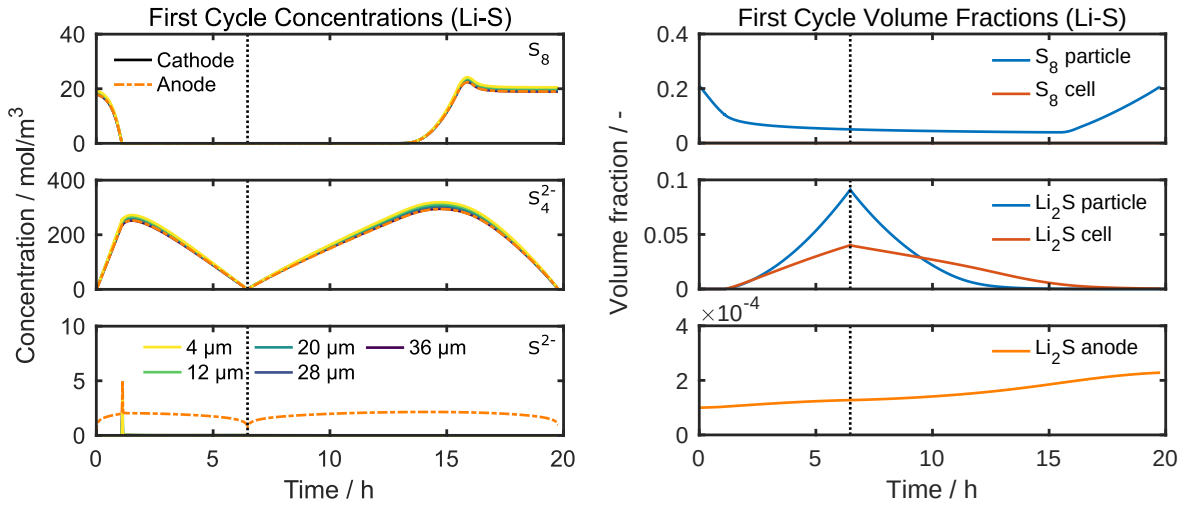

(a) (b)

Figure 3: a) average concentration inside cathode particles (solid lines) and at the anode surface (dashed lines). The color code of the cathode concentrations relates to the color legend as introduced in Fig. 1 on the x-axis of Fig. 1. The anode concentration given by the orange region in Fig. 1 is given by the dashed orange line. b) the first two panels show the volume fractions during the first cycle of a Li-S battery in the cathode domain. The solid blue and red lines indicate the phase distribution inside the particles and on the particle surface following the color coding introduced in Fig. 1. The lower panel shows the volume fraction at the anode (cf. orange region of Fig. 1) of the cell model. The vertical dotted line denotes the transition from discharge to charge.

capacity loss.

One aspect, which will receive more attention in the paragraphs below, is the concentration gradient along the x-axis caused by the polysulfide shuttle. This gradient has a direct effect on dissolution and deposition processes in the cell and will be discussed in detail in Sections 3.3 and 3.4.

3.1.2 Mg-S cell

Electrochemical characterization Fig. 2 b) shows the experimental and simulated charge and discharge curves of Mg-S batteries. Typically only half of the theoretical capacity is reached during discharge of Mg-S batteries. This capcaity loss can be perfectly reproduced in our simulations by including the effects of the polysulfide shuttle mechanism.

In the Mg-S battery simulations we model nucleation and growth of solid phases in the same way as in Li-S batteries. Still, we do not see a feature in the cell voltage at the beginning of the second plateau. This is in qualitative agreement with the experiments where this nucleation dip also cannot be observed. In the literature there is some debate if formation of solid phases, in particular MgS or MgS_2 occurs in Mg-S batteries.[23,33] Our simulations demonstrate that formation of solid discharge products is possible despite the missing characteristic feature in the cell voltage. Precipitation of other polysulfide species such as MgS_4 has not been reported in the literature. We will discuss this effect in more detail in the paragraph below.

In comparison to our previous work[21] the position of the second plateau is in qualitative agreement with the experimental data. Based on our storage experiments at OCV we determined an equilibrium potential of the second plateau to around 1.1 V. During the C/10 discharge the cell voltage is lower in the second plateau indicating a significant overpotential due to sluggish kinetics of the electrochemical reactions. In our simulations we take this effect into account by using a low frequency factor for corresponding reactions.

Again, the voltage step between the upper and lower plateau is much more pronounced in our simulations compared to the experiments. Still, the length and the voltage of the two plateaus,

as well as the overall discharge capacity, are in good agreement with the experimental data.
During battery charge the differences between experiments and simulations are much more distinct. As a result, we do not reach the voltage level at which the experiment switches from CC to CV. To be able to reproduce the experiment as accurately as possible, we switch in our simulations to CV operation (dashed line) after reaching the highest voltage. This procedure is also used in the further course. Additionally, we include simulations with a constant current (CC) protocol (solid line) in Fig. 2 b)
However, this indicates that the reactions during charge are much slower compared to discharge, which might be attributed to the formation of solid degradation products or additional side reactions. This is also in line with one of our previous studies on the polysulfide shuttle in Li-S batteries.[22] Another possibility is the passivation of the Mg surface due to solid reaction products or the desolvation of Mg-ions during plating. We investigate this process at the end of this section.

Concentration and phase distribution
Fig. 4 a) and b) show the concentrations of dissolved species and volume fractions of solid phases in the initial cycle. During discharge qualitative trends of $S_8^{(l)}$ and S_4^{2-} concentrations are very similar to Li-S batteries discussed in Section 3.1.1. Although the S_4^{2-} concentration is slightly higher in the Mg-S battery the order of magnitude is quite similar. In the literature solubility data of polysulfides is relatively scare. However, in some sources solubilities of up to 250 mol/m^3 are reported. This is close to values simulated here and as discussed above our concentrations are representative for several longer polysulfides. Therefore, we are not able to draw a final conclusion on the precipitation of intermediate species along the reaction chain and neglect any precipitation. Nevertheless, in the supporting information in Sec. 8, we address this issue and highlight possible effects. However, the S^{2-} concentration clearly shows different behavior, which can be explained by the much more pronounced polysulfide shuttle. During the upper discharge plateau we observe higher S^{2-} concentrations which are identical at the anode and cathode. In this stage reduction to S^{2-} occurs only by side reactions at the anode surface. Even before the cell voltage drops to the lower plateau we see a minimum in S^{2-} concentration due to the precipitation of MgS. The complex concentration evolution of S^{2-} can be explained by nucleation and growth kinetics, which was described in detail in our previous publication.[21]
In contrast to the Li-S system, the major amount of MgS precipitates uniformly in the particles and on the particle surface during the lower plateau. A detailed analysis is given in Sec. 3.4. At the anode the fast kinetics of the side reactions cause a much stronger precipitation of MgS compared to Li_2S in the Li-S battery.
While in the upper plateau the concentration of S^{2-} in the cathode and at the anode are similar, differences can be seen in the lower plateau. This can be explained by the consumption of S^{2-} due to fast precipitation of MgS at the anode causing a relatively thick film on the Mg surface.
During charge the parasitic side reactions prevent hardly any oxidation of polysulfide species at the cathode. This process, eventually causing the infinite charging phenomenon, can be explained by analyzing the concentrations and volume fractions. Continuous reduction of dissolved polysulfides on the Mg surface causes a constant precipitation of MgS at the anode. As discussed above for the Li-S system, this causes irreversible loss of active material. On the other hand, concentrations of longer polysulfides build up very slowly. Therefore, only a small amount of $S_8^{(s)}$ precipitates in the cathode. Fig. S5 shows the volume fractions of S_8 in even more detail. However, in contrast to the Li-S system, this precipitation occurs uniformly in the particles and on the particle surface (see Sec. 3.3). After 8 hours of CV phase the cell is still not fully charged. In our simulations we still see a relevant concentration of S_4^{2-} species, as well as some residual MgS in the cathode.
Similar to Li-S batteries we see small concentration gradients for all species across the cell thickness causing a redistribution of sulfur

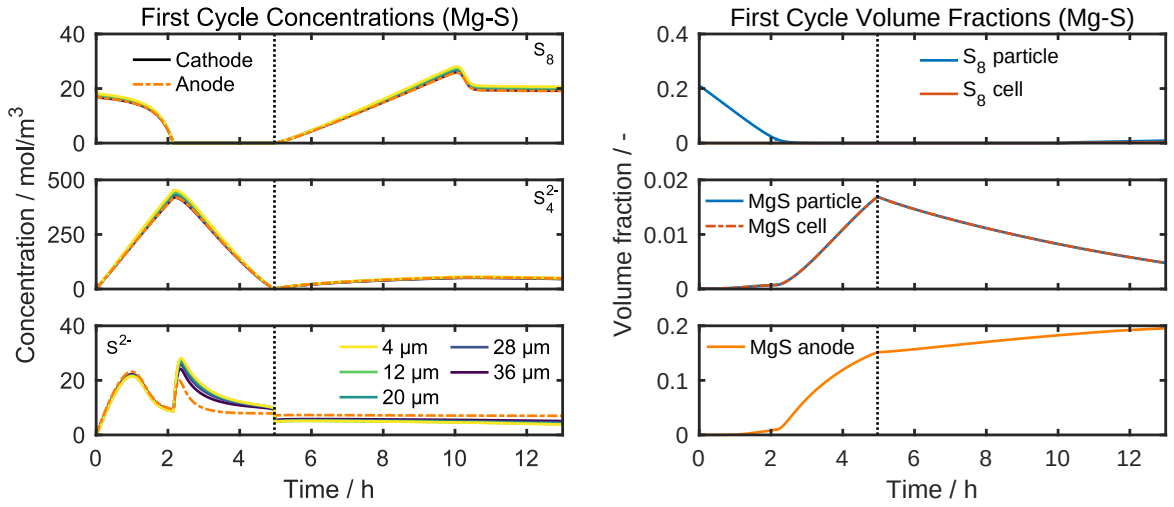

(a) **(b)**

Figure 4: a) average concentrations inside cathode particles (solid lines) and at the anode surface (dashed lines). The color gradient of the cathode concentrations relates to the color gradient on the x-axis of Fig. 1. Similarly, the anode concentration of the orange region of Fig. 1 is shown. b) the first two panels show the volume fractions during the first cycle of a Li-S battery within the cathode for the particle and cell model as described in Sec. 2.2. The lower panel shows the volume fraction at the anode (see orange region of Fig. 1) of the cell model. The vertical dotted line denotes the transition from discharge to charge.

species. A more detailed discussion of this effect is given in the following sections.

Anode passivation As outlined above the anode is of central importance for Me-S systems. While limiting processes in the cathode definitely deserve more research, several sources in the literature report that the low coulombic efficiency of the cells can be mainly attributed to the anode kinetics.[24,34] Therfore, a detailed model for anode processes is needed, especially for Mg based battery chemistries.[35,36] Chadwick *et al.*[37] are the first to report a continuum model for plating and stripping of Mg. They found a symmetry factor for the reaction of only 0.1 resulting in preferential stripping of Mg. This observation is in line with generally higher overpotentials during battery charge. However, in our simulations adjusting α had only a minor effect on the charging voltage. The corresponding results can be found in Fig. S3. This indicates that the sulfur species on the electrode surface amplify kinetic limitations during battery charge. This is in line with experimental data in the literature.[4,5,8]

It is generally accepted that MgS and other side products are insulating materials. Therefore, the formation of solid phases passivates the metal surface. To correlate the simulated volume fractions with the active surface area we provide here a first phenomenological model considering the passivation of the magnesium surface by MgS.[14] Note, that this blocking layer of MgS can be regarded as representative for the effect of other insulating side products on the Mg metal surface. This phenomenological expression is based on our previous work[22]

$$f(\varepsilon_{\mathrm{MgS}}) = \left(\frac{\varepsilon_{\mathrm{MgS,block}} - \varepsilon_{\mathrm{MgS}}}{\varepsilon_{\mathrm{MgS,block}}} \right), \tag{1}$$

where $\varepsilon_{\mathrm{MgS,block}}$ and $\varepsilon_{\mathrm{MgS,solid}}$ are the limiting and simulated volume fraction of MgS, respectively. Typically, the maximum distance for electron tunneling corresponding to a limiting film thicknes is in most materials around 2-3 nm. This is also in line with studies on various SEI materials in lithium based batteries.[13] Therfore, we can safely assume passivation of the surface if the thickness exceeds 4 nm corresponding to 9 layers of MgS molecules.[38] The volume fraction of MgS can be converted to a layer thickness taking into account surface roughness and ho-

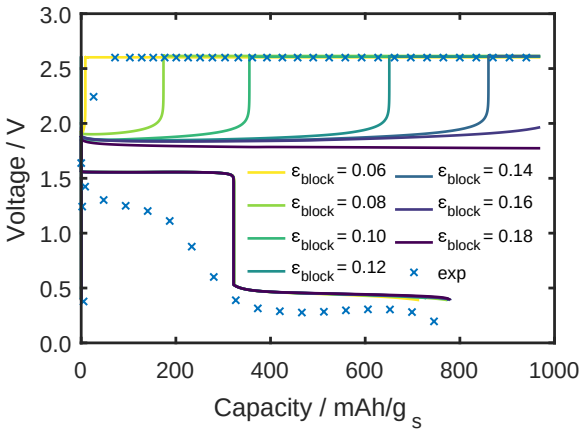

Figure 5: Influence of a blocking anode surface with different values for $\varepsilon_{\text{block}}$ of equation 1.

mogeneity of the deposits. For a uniform film on a perfectly smooth surface the limiting volume fration in our simulations is $\varepsilon_{\text{block}} = 8 \cdot 10^{-4}$. To investigate the effect of inhomogeneous deposits and increasing surface roughness due to plating and stripping of Mg we perform charging simulations with different limiting volume fractions $\varepsilon_{\text{block}}$. A sumary of the results can be found in Fig. 5.

Generally, we see only a minor influence of the anode passivation on the discharge capacity. Similarly, for $\varepsilon_{\text{block}}$ larger than 0.18 the passivation of the surface area has barely any effect on the charge process. However, with decreasing limiting volume fraction the cell voltage reaches the upper cut-off voltage at 2.6V and the charge process continues with the CV phase. At very small $\varepsilon_{\text{block}}$ the cell voltage immediately jumps to 2.6V and we can report qualitative agreement with the experimental data given by blue crosses in Fig. 5. This indicates that $\varepsilon_{\text{block}}$ between 0.06 to 0.08 is a suitable range for this phenomenological parameter. Below $\varepsilon_{\text{block}}$=0.06 charging of the battery at C/10 is not possible due to complete passivation of the surface.
Note, that the parameter range discussed above is around two orders of magnitude larger than the estimated limiting volume fraction for uniform deposits on a smooth surface. This indicates that it is important to study the morphology of the Mg surface, including the structural properties of the deposits, the surface roughness, and partial surface activation or deactivation, respectively. Moreover, advanced models to study the processes on the Mg metal surface need to be developed which is also in the focus of our activities.[39]

3.2 Cycling and cell degradation

In addition to the first cycle shown in Sec. 3.1 we also study the cycling behavior of Li-S and Mg-S batteries. We pay specific attention to the first 10 cycles which are shown in Fig. 6. In both systems, experimentally, as well as in the simulations, we observe a strong decrease in capacity compared to the first cylce which will be analyzed in the following paragraphs.

3.2.1 Li-S cell

Fig. 6 a) shows simulated discharge curves of the first 10 cycles of a Li-S battery. The simulated loss in capacity over 10 cycles is in good agreement with the experimental data. Our simulations confirm that the anticipated loss of active sulfur from the cathode in an irreversible precipitation reaction of Li_2S at the anode surface can be one reason for the capacity fading. The increasing volume fractions of Li_2S on the anode surface is shown in Fig. 7 a). The precipitation of the solid phase ist almost continuous during discharge and charge. It only stops at the very end of the charging process when all sulfur species are almost completely oxidized. In this case the side reactions at the anode are too slow to supply a significant amount of S^{2-}. This leads to a slow but almost continuous growth of Li_2S on the anode surface resulting in a moderate capacity fade during cycling.
Interestingly the length of the first plateau is almost constant while the length of the second plateau gradually decreases. Our simulations suggest that the stability of the first plateau is due to a redistribution of active sulfur within the cathode towards the current collector. This effect results in a suppression of the polysulfide shuttle during the first plateau. However, it should be mentioned that the upper plateau in the first cycle of our experiments is somewhat shorter compared to the following cycles. Most

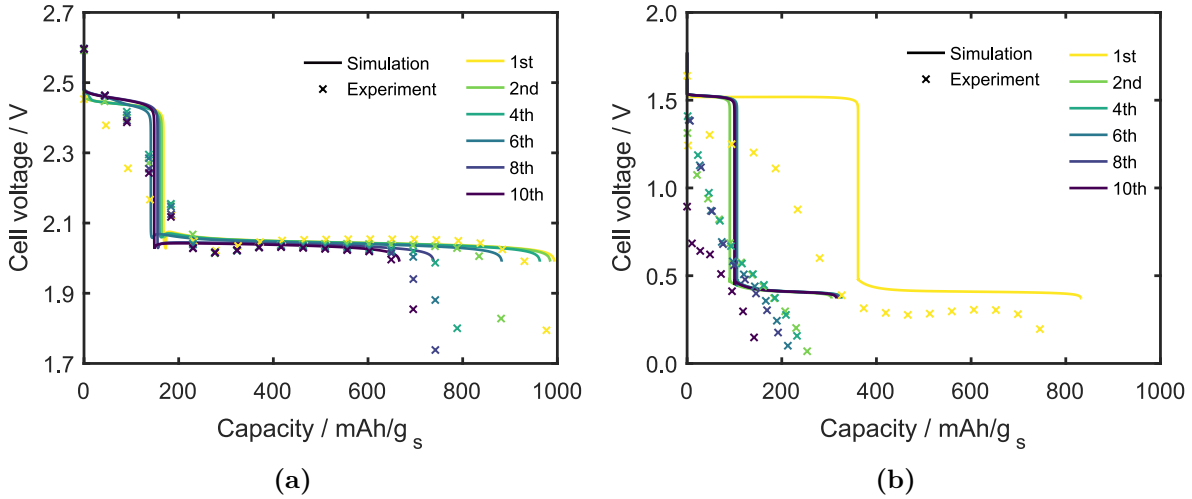

Figure 6: Comparison of experimental and simulated discharge behavior at C/10. Every second discharge from 1st to 10th is shown for representative a) Li-S and b) Mg-S cells.

likely the battery has not been completely equilibrated after the short rest period of only one hour following cell assembly. The redistribution of active sulfur is discussed in more detail in section 3.3.

3.2.2 Mg-S cell

For the Mg-S system the discharge curves of the first 10 cycles are shown in Fig. 6 b). Again, some agreement can be seen between the simulation and the experiment. However, it is not as good as with the Li-S system shown previously. While the rapid drop in capacity between the first and second cycle is well reproduced, other features cannot be represented by the model. In the experiment, the capacity continues to decrease after the second cycle, albeit at a much slower rate. In the simulations the discharge capacity stabalizes and we observe only minor capacity fade. The change in the shape of the discharge curve, which can be seen in the experiment, is also not reproduced by the model. One plausible explanation is that in the experiment the fast polysulfide shuttle suppresses the formation of any solid sulfur which is still observed to some extent in our simulations. Therefore, the upper plateau is very short before it vanishes completely. On the one hand, side reactions not described by the model may be responsible for this. However, it is also possible that the reason for this is the simplified reaction pathway used in the model, whereby species belonging to the upper plateau are formed directly during charge, whereas species of the lower plateau are formed first in the experiment.

However, an important reason for the dramatic loss of capacity from first to second cycle is the incomplete re-oxidation of sulfur during charge due to the pronounced polysulfide shuttle. The corrsponding concentration profiles are discussed in Section 3.1. This causes qualitatively different kinetics for the formation of solid degradation products on the metal surface in Li-S and Mg-S batteries, respectively (cf. Fig. 7). While we simulate a slow but continuous growth of Li_2S in Li-S batteries, our simulations predict a rapid irreversible growth of MgS during the first cycle in Mg-S batteries. In subsequent cycles the average volume fraction is rather constant around 0.3 and we see only minor growth during discharge and dissolution during charge. Since there is no continuous growth of the film on the anode, as in the case of the Li-S battery, it is clear why a rapid drop in capacity is only observed between the first and second cycle. Further loss of capacity due to growth of MgS on the anode is at least not observed in the simulations. However, it is very likely that further, albeit greatly reduced, precipitation of MgS occurs in the experiment providing another explanation for the continuous loss of capacity. Furthermore, in comparison to the Li-S system

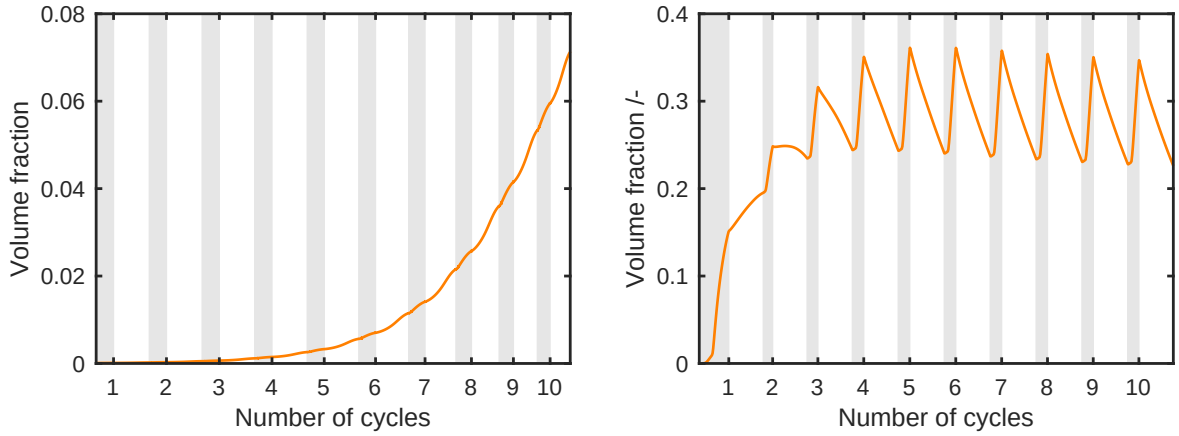

(a) **(b)**

Figure 7: Comparison of the solid discharge product Li_2S and MgS at the Anode. a) Li_2S and b) MgS. The shaded areas show the discharge phases whereas the unshaded areas show the charging phases.

the length of the first plateau also decreases after the first cycle. Although a redistribution of sulfur takes place in a similar way as in the Li-S system, this is not sufficient to compensate the polysulfide shuttle. This effect is also discussed in more detail in Section 3.3.

3.3 Sulfur redistribution

In addition to the formation of solid phases on the anode surface, the polysulfide shuttle also affects the local composition and electrolyte concentrations in the cathode. In particular, we discuss in this section the spatial redistribution of active sulfur in the cathode and its impact on electrochemical performance and cycle life.

3.3.1 Li-S cell

As shown in Fig. 6 a) the length of the first plateau of the Li-S battery discharge curve remains the same during cycling while the overall discharge capacity decreases. Fig. 8 a) and b) show the spatial distribution of the simulated volume fraction of solid sulfur in the cathode along the x-axis in the particles and on the particle surfaces, respectively. Starting with a homogeneous distribution throughout the electrode the simulations predict a redistribution of sulfur during battery charge. As shown in Fig. 8 a) we observe higher volume fractions of sulfur within particles close to the cathode current collector after recharging the battery. The reason for this, is the aforementioned concentration gradient of dissolved polysulfides due to an external current as shown in Fig. 3. Higher polysulfide concentrations close to the cathode current collector favor the inhomogeneous precipitation of sulfur.
As a result the average diffusion length of residual polysulfide species increases during cycling. As indicated above this effect mitigates the polysulfide shuttle. Still, we observe a reduction of the average sulfur volume fraction within cathode particles which becomes pronounced after the fifth cycle. This increased utilization of sulfur compensates the capacity loss due to the precipitation at the anode and leads to a stable length of the first plateau. With increasing cycle number we expect that the precipitation on the anode will also reduce the first plateau. The exponential growth of Li_2S on the anode surface as seen in Fig. 7 a) also points in this direction. Another interesting observation is that our model predicts negligible precipitation of S_8 on the particle surface as seen in Figure 8 b). This is due to the incomplete utilization of sulfur during discharge. In our model the growth of existing sulfur clusters is favored compared to nucleation of new clusters on the carbon matrix. This effectively suppresses the precipitation of sulfur on the particle surface. Therefore, the solid sulfur confined within the particle pores

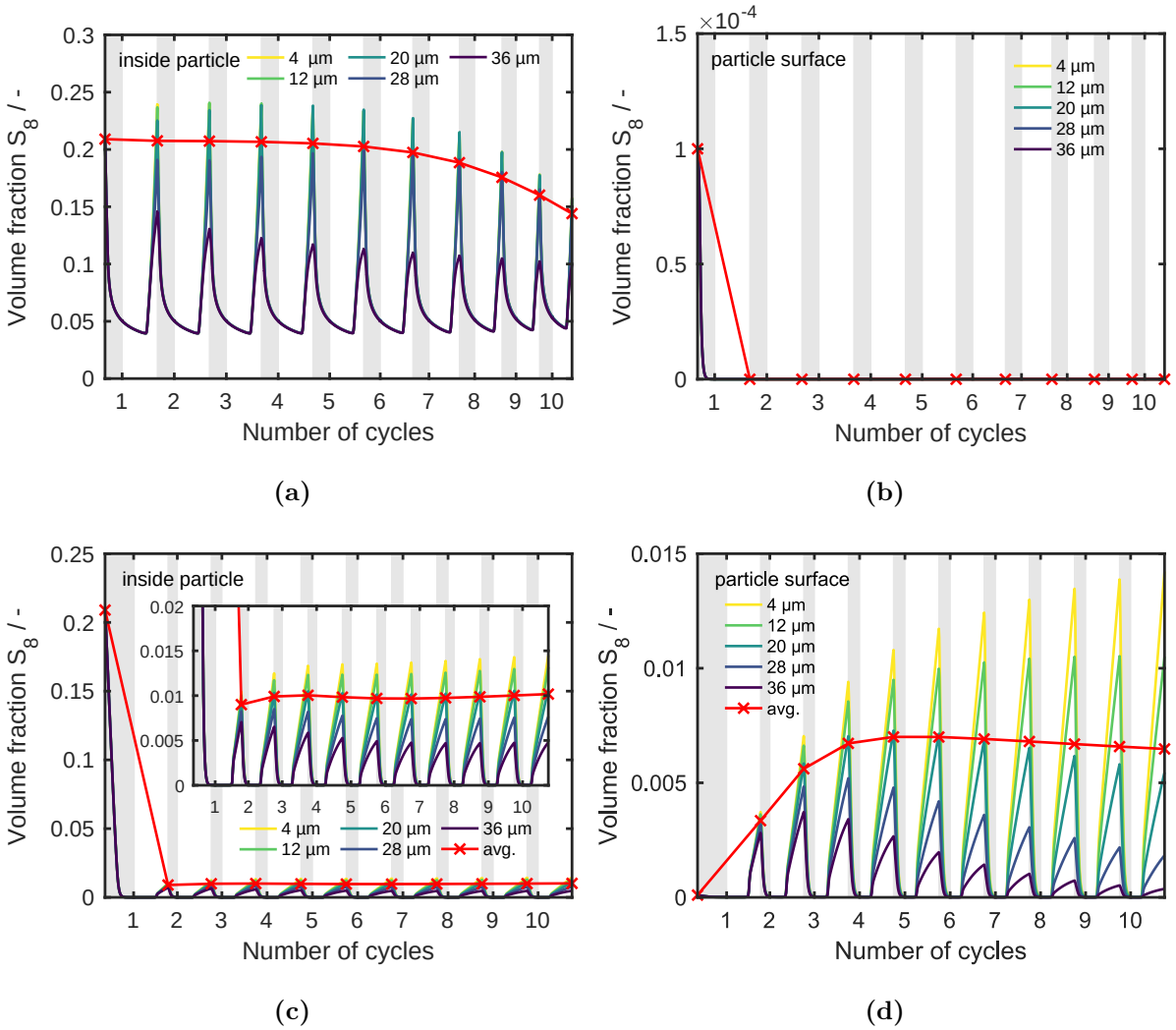

Figure 8: Comparison of simulated volume fractions of S_8. a) and b) show the volume fractions inside (blue line in Fig. 1) and on the particle surfaces (red line in Fig. 1) of the Li-S system and c) and d) show the volume fractions inside and on the particle surfaces of the Mg-S system, respectively. The solid red line indicates the average volume fraction at the beginning of discharge. Distances are given from the cathode current collector along the x-axis in direction of the separator. The shaded areas show the discharge phases whereas the unshaded areas show the charging phases.

contributes to the long term stability of the Li-S cell.

3.3.2 Mg-S cell

Fig. 8 c) and d) show the simulated distribution of solid sulfur volume fraction of solid sulfur in the cathode particles and on the particle surfaces in a Mg-S battery. The most important information in Fig. 8 c) is the rapid loss of sulfur to the macroscopic pore space and the very low sulfur precipitation within particles during charge. The polysulfide shuttle prevents re-oxidation of sulfur during charge and only a small amount of S_8 is able to form. This contributes to the strong capacity fading during cycling as discussed in 3.2.

Similar to the Li-S system our simulations predict a redistribution of solid sulfur as a result of the concentration gradient of dissolved polysulfide species.

Another distinctive difference between Li-S and Mg-S cells is the formation of sulfur on the particle surface. Due to the full dissolution of sulfur within the particles as seen in Fig. 8 c) no peferential nucleation sites remain inside particle micropores. Therefore, we see comparable volume fractions in the particles and on their

surface as shown in Fig. 8 c) and d). Note, that precipitation on the surface of the particles is increasing in the first cycles before the polysulfide shuttle consumes an increasing share of the sulfur inventory. Analoguos to the inhomogeneous sulfur distribution in x-direction within the particles we observe that mainly sulfur close to the separator contributes to this loss mechanism.
In order to provide a better picture for the redistribution we calculate the corresponding layer thickness of sulfur for some simulated volume fractions in the particles and on the particle surface. For example, at the beginning of the first cycle, when all S_8 is in the pores of the particles, the thickness of a uniform layer in the pores is about 1 nm. At the beginning of the second discharge, however, the layer thickness in the particles is only around 0.05 nm. On the particle surfaces, in contrast, a layer thickness of up to 10 nm of solid sulfur forms after a few cycles. However, in the experiments sulfur particles form instead of uniform sulfur layers[40] if non uniform morphologies or particles are observed. Therefore, the expected particle sizes are larger than the thickness of uniform layers calculated here.[32]

3.4 Discharge product distribution

To reduce the shuttle effect a precipitation of discharge products inside the particles is preferable. In our study we do not use functionalized materials and we do not expect preferential nucleation sites within the cathode or even within cathode particles. Therefore, the formation of precipitate depends only on the solubility and distribution of dissolved polysulfides. As already discussed in section 3.3 the concentration of polysulfides is strongly influenced by the polysulfide shuttle and the effect on spatial distribution of discharge products will be discussed below.

3.4.1 Li-S cell

Fig. 9 a) and b) show the simulated volume fractions of Li_2S inside cathode particles and on the particle surface, respectively. By comparing the average volume fraction of Li_2S inside the particles and on the particle surfaces it is apparent, that most of the Li_2S indeed precipitates inside the particles. The dissolution of sulfur, also during the second plateau, provides a continuous supply of dissolved polysulfides inside the particles. The polysulfides are reduced directly within the particles and precipitate on the walls of the micropores. Therefore, only smaller amounts of polysulfides are able to leave the particles, reducing the precipitation of Li_2S on the particle surface.
Additionally, we observe an inhomogeneous precipitation of Li_2S on the particle surface (cf. Fig. 9 b)). The polysulfide shuttle provides a continuous supply of S^{2-} from the anode surface as shown for the first cycle in Fig. 3 a). Even at the beginning of charge the amount of Li_2S increases near the separator due to polysulfides from the anode. During the first discharge this supply causes a higher amount of Li_2S in the cathode particles and on the particle surfaces near the separator.

3.4.2 Mg-S cell

The distribution of discharge products in Mg-S cells is very different compared to the distributions in Li-S cells discussed above. The volume fractions of MgS inside the particles and on the particle surfaces are shown Fig. 9 c) and d), respectively. Due to the fast dissolution of sulfur there is no comparable mechanism which promotes MgS precipitation inside the particles. Therefore, we observe almost the same average amount of MgS inside the particles and on particle surfaces during discharge. Moreover, since the side reactions on the anode surface consume a significant share of the active sulfur, the overall amount of MgS also reduces. Almost no precipitation of MgS is visible after the fourth cycle.
Additionally, our simulations predict a significant spatial gradient of MgS along the x-axis. This gradient, however, is opposite to the gradient of Li_2S observed in Li-S batteries. This is due to the fast consumption of S^{2-} in the side reactions at the Mg surface. Consequently, we observe lower S^{2-} concentrations at the anode current collector than in the cathode (cf. Fig.

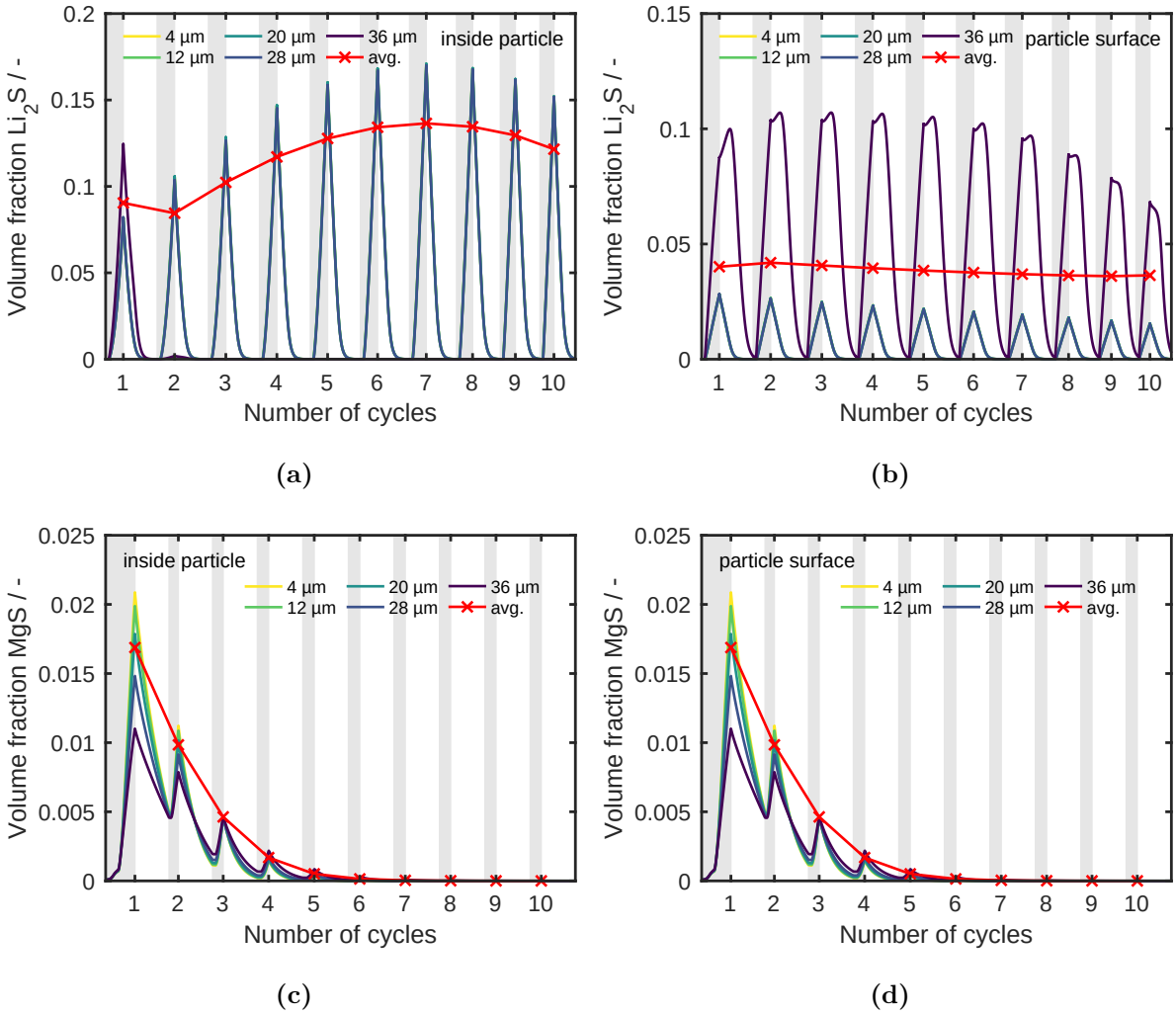

Figure 9: Comparison of the solid discharge product Li_2S and MgS. a) Li_2S inside the particles (blue line in Fig. 1), b) Li_2S on the particle surfaces (red line in Fig. 1), c) MgS inside the particles d) MgS on the particle surfaces. The red solid line indicates the average volume fraction at the end of discharge. Distances are given from the cathode current collector along the x-axis in direction of the separator. The shaded areas show the discharge phases whereas the unshaded areas show the charging phases.

4 a)). This causes a flux of S^{2-} to the anode and higher MgS volume fractions close to the cathode current collector.

3.5 Increased sulfur loading

The motivation of our work is to provide theoretical tools for the development and commercialization of Me-S batteries. Therefore, we want to bridge the gap between cells used in research and academia and design targets for commercialization. An important parameter for the commercialization of Me-S batteries is the sulfur loading of the composite cathode. In order to provide predictions for cells closer to commercialization we increase the sulfur loading in our simulations from 0.75 mg cm^{-2} to 1.5 mg cm^{-2}. Although this is a significant increase in sulfur loading we have to mention that at least 3 mg cm^{-2} are needed to be competitive to Li-Ion batteries.

The particles of the carbon materials in our studies exhibit a porosity of 80 vol-%. The sulfur volume fraction of 20 vol-% corresponds to the aforementioned sulfur loading of 0.75 mg cm^{-2}. Theoretically, this leaves room for much higher sulfur concentrations within the particles. Since the energy density is crucial for practical applications we increase the sulfur loading in our simulations to 40 vol-% on particle level

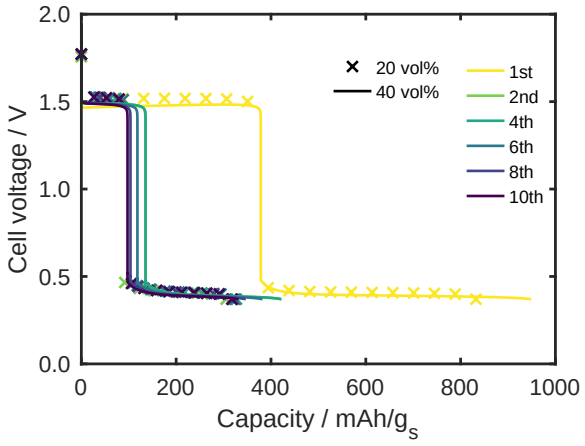

Figure 10: Comparison of the first 10 cycles of a simulated Mg-S battery with a sulfur loading of 40 vol% to the simulation results with a sulfur loading of about 20 vol%.

corresponding to our design target of 1.5 mg cm^{-2}. The thickness of the cathode remains unchanged.

Fig. 10 shows the first ten cycles charge and discharge curves of a Mg-S battery with a loading of 1.5 mg cm^{-2} . Simulation results of our standard setup are also included as dashed line for reference. In the simulations the external currents are adjusted to the sulfur loading and in both cases we use a C/10 rate.

Due to the higher currents the cell voltage is a few mVs lower in the cell with higher sulfur loading. An increased sulfur loading would also lead to a lower electrical conductivity and thus increase the overvoltage. Interestingly, the capacity in the first cycles even increases showing a beneficial effect of higher sulfur loadings and corresponding currents.

The reason for the initial increase in discharge capacity is that the increase in sulfur reduces the electrolyte volume. Therefore, during discharge, concentrations of dissolved species increase faster, resulting in earlier precipitation of MgS and thus increased nucleation seeds. This leads to a suppression of the shuttle effect. It can also be assumed that the higher currents compared to the lower loading help to suppress the shuttle effect. It is also possible that higher sulfur loading leads to more nucleation sites during cycling due to incomplete dissolution. However, at least in our simulations, we did not observe this effect. Fig. S6 shows that even with an increased sulfur loading, complete dissolution of the sulfur takes place in our simulations.

However, this advantage reduces in subsequent cycles. Still, it is important to notice that higher sulfur loadings do not seem to have a negative effect on the cycle life. This is a promising first result for the upscaling of the technology since the corresponding volumetric capacities of electrodes with high sulfur loadings outperform the electrodes with lower sulfur content (cf. Fig. 10). Future studies in novel electrolyte systems will be performed to shed some more light in this topic.

4 Conclusion

Me-S batteries are promising candidates for the next generation of batteries. We want to contribute to this development by providing advanced models for analysis of electrochemical measurements and design of new electrode and cell geometries.

In our modeling framework for Li-S and Mg-S batteries we explicitly take into account the polysulfide shuttle including side reactions at the anode surface. By comparing to experimental data we are able to demonstrate qualitative agreement between simulations and measurements of Li-S and Mg-S batteries within the first 10 cycles.

In a next step we use our model to analyze the charge and discharge process. Our simulations indicate that side reactions and the formation of passivating films on the Mg surface in Mg-S batteries cause large overpotentials during charge. We provide a first phenomenological model for surface passivation to investigate this effect. The results show that more sophisticated models and surface analysis are needed to resolve the origin of the extremely high overpotentials.[6,14,30,33,34]

Furthermore, we investigated the redistribution of sulfur species during cycling. In Li-S batteries we found that undissolved sulfur, which is undesirable due to lower capacities, can act as precipitation center during charge and improves the cycle life of the battery.

In agreement with our previous study we con-

clude that side reactions are dominant in Mg-S batteries with $Mg(HMDS)_2$-$AlCl_3$ electrolytes and cause very poor cycling stability. Specifically, we see that infiltrated sulfur rapidly leaves the host structure and causes significant film growth on the Mg surface. Moreoever, the polysulfide shuttle prevents complete oxidation of sulfur species in the electrolyte during charge. Finally, we demonstrate application of our model for the development of sulfur-carbon composite cathodes with suitable sulfur loadings for commercial applications. Our simulations indicate that higher sulfur loadings might actually be beneficial for the capacity density of Mg-S cells without compromising the cycle life. Still, the capacity decay in our simulations is significant and the sulfur loading is still too low for most applications. Improvements from material to cell level are needed to make Mg-S batteries competitive with state-of-the-art battery technologies.

Acknowledgement This work has received funding from the German Federal Ministry for Education and Research (BMBF) under grant agreement No 03XP0032A (MagS). Furthermore, this work contributes to the research performed at CELEST (Center for Electrochemical Energy Storage Ulm-Karlsruhe).

Supporting Information Available

The following files are available free of charge.

- Supporting Information.pdf: Reaction mechanism, model equations, List of parameters, comparison of current parameters with those from previous work, effect of unequal symmetry factor of Mg plating and stripping, additional particle and cell concentrations.

References

(1) Peled, E.; Gorenshtein, A.; Segal, M.; Sternberg, Y. Rechargeable lithium-sulfur battery. *Journal of Power Sources* **2003**, *26*, 269–271.

(2) Bruce, P. G.; Freunberger, S. A.; Hardwick, L. J.; Tarascon, J. M. LigO2and LigS batteries with high energy storage. *Nature Materials* **2012**, *11*, 19–29.

(3) Zhao-Karger, Z.; Behm, R. J.; Zhao, X.; Wang, D.; Fichtner, M.; Diemant, T. Performance Improvement of Magnesium Sulfur Batteries with Modified Non-Nucleophilic Electrolytes. *Advanced Energy Materials* **2015**, *5*, 1401155.

(4) Wang, Z.; Wang, X.; Sun, W.; Sun, K. Dendrite-Free Lithium Metal Anodes in High Performance Lithium-Sulfur Batteries with Bifunctional Carbon Nanofiber Interlayers. *Electrochimica Acta* **2017**, *252*, 127 – 137.

(5) Tarascon, J. M.; Armand, M. Issues and challenges facing rechargeable lithium batteries. *Nature* **2001**, *414*, 359–367.

(6) Jäckle, M.; Groß, A. Microscopic properties of lithium, sodium, and magnesium battery anode materials related to possible dendrite growth. *Journal of Chemical Physics* **2014**, *141*.

(7) Ling, C.; Banerjee, D.; Matsui, M. Study of the electrochemical deposition of Mg in the atomic level: Why it prefers the non-dendritic morphology. *Electrochimica Acta* **2012**, *76*, 270–274.

(8) Kim, H. S.; Arthur, T. S.; Allred, G. D.; Zajicek, J.; Newman, J. G.; Rodnyansky, A. E.; Oliver, A. G.; Boggess, W. C.; Muldoon, J. Structure and compatibility of a magnesium electrolyte with a sulphur cathode. *Nature Communications* **2011**, *2*, 426–427.

(9) Xiong, S.; Xie, K.; Diao, Y.; Hong, X. Characterization of the solid electrolyte interphase on lithium anode for preventing the shuttle mechanism in lithium-sulfur batteries. *Journal of Power Sources* **2014**, *246*, 840–845.

(10) Bresser, D.; Passerini, S.; Scrosati, B. Recent progress and remaining challenges in sulfur-based lithium secondary batteries - a review. *Chemical Communications* **2013**, *49*, 10545–10562.

(11) Zhang, S. S. Liquid electrolyte lithium/sulfur battery: Fundamental chemistry, problems, and solutions. *Journal of Power Sources* **2013**, *231*, 153–162.

(12) Zhu, Y.; Wang, S.; Miao, Z.; Liu, Y.; Chou, S. L. Novel Non-Carbon Sulfur Hosts Based on Strong Chemisorption for Lithium-Sulfur Batteries. *Small* **2018**, *14*, 1–21.

(13) Wang, A.; Kadam, S.; Li, H.; Shi, S.; Qi, Y. Review on modeling of the anode solid electrolyte interphase (SEI) for lithium-ion batteries. *npj Computational Materials* **2018**, *4*.

(14) Salama, M.; Attias, R.; Hirsch, B.; Yemini, R.; Gofer, Y.; Noked, M.; Aurbach, D. On the Feasibility of Practical Mg–S Batteries: Practical Limitations Associated with Metallic Magnesium Anodes. *ACS Applied Materials & Interfaces* **2018**, *10*, 36910–36917, PMID: 30295459.

(15) Yoo, H. D.; Shterenberg, I.; Gofer, Y.; Gershinsky, G.; Pour, N.; Aurbach, D. Mg rechargeable batteries: an on-going challenge. *Energy Environ. Sci.* **2013**, *6*, 2265–2279.

(16) Aurbach, D.; Weissman, I.; Gofer, Y.; Levi, E. Nonaqueous magnesium electrochemistry and its application in secondary batteries. *The Chemical Record* **2003**, *3*, 61–73.

(17) Wang, P.; Buchmeiser, M. R. Rechargeable Magnesium–Sulfur Battery Technology: State of the Art and Key Challenges. *Advanced Functional Materials* **2019**, *29*, 1905248.

(18) Zhao-Karger, Z.; Fichtner, M. Magnesium-Sulfur battery: its beginning and recent progress. *MRS Communications* **2017**, *7*, 770–784.

(19) Thangavel, V.; Xue, K.-H.; Mammeri, Y.; Quiroga, M.; Mastouri, A.; Guéry, C.; Johansson, P.; Morcrette, M.; Franco, A. A. A Microstructurally Resolved Model for Li-S Batteries Assessing the Impact of the Cathode Design on the Discharge Performance. *Journal of The Electrochemical Society* **2016**, *163*, A2817–A2829.

(20) Danner, T.; Zhu, G.; Hofmann, A. F.; Latz, A. Modeling of nano-structured cathodes for improved lithium-sulfur batteries. *Electrochimica Acta* **2015**, *184*, 124–133.

(21) Richter, R.; Häcker, J.; Zhao-Karger, Z.; Danner, T.; Wagner, N.; Fichtner, M.; Friedrich, K. A.; Latz, A. Insights into Self-Discharge of Lithium– and Magnesium–Sulfur Batteries. *ACS Applied Energy Materials* **2020**, *3*, 8457–8474.

(22) Hofmann, A. F.; Fronczek, D. N.; Bessler, W. G. Mechanistic modeling of polysulfide shuttle and capacity loss in lithium-sulfur batteries. *Journal of Power Sources* **2014**, *259*, 300–310.

(23) Robba, A.; Vizintin, A.; Bitenc, J.; Mali, G.; Arčon, I.; Kavčič, M.; Žitnik, M.; Bučar, K.; Aquilanti, G.; Martineau-Corcos, C.; Randon-Vitanova, A.; Dominko, R. Mechanistic Study of Magnesium-Sulfur Batteries. *Chemistry of Materials* **2017**, *29*, 9555–9564.

(24) Vinayan, B. P.; Euchner, H.; Zhao-Karger, Z.; Cambaz, M. A.; Li, Z.; Diemant, T.; Behm, R. J.; Gross, A.; Fichtner, M. Insights into the electrochemical processes of rechargeable magnesium–sulfur batteries with a new cathode design. *J. Mater. Chem. A* **2019**, *7*, 25490–25502.

(25) Gao, T.; Ji, X.; Hou, S.; Fan, X.; Li, X.; Yang, C.; Han, F.; Wang, F.; Jiang, J.; Xu, K.; Wang, C. Thermodynamics and Kinetics of Sulfur Cathode during Discharge

in MgTFSI 2 -DME Electrolyte. *Advanced Materials* **2017**, *30*, 1704313.

(26) Xu, Y.; Ye, Y.; Zhao, S.; Feng, J.; Li, J.; Chen, H.; Yang, A.; Shi, F.; Jia, L.; Wu, Y.; Yu, X.; Glans-Suzuki, P.-A.; Cui, Y.; Guo, J.; Zhang, Y. In Situ X-ray Absorption Spectroscopic Investigation of the Capacity Degradation Mechanism in Mg/S Batteries. *Nano Letters* **2019**, *19*, 2928–2934, PMID: 30932498.

(27) Kumaresan, K.; Mikhaylik, Y.; White, R. E. A Mathematical Model for a Lithium-Sulfur Cell. *Journal of The Electrochemical Society* **2008**, *155*, A576.

(28) Su, L.; Ferrandon, M.; Barton, J. L.; de la Rosa, N. U.; Vaughey, J. T.; Brushett, F. R. An investigation of 2,5-di-tertbutyl-1,4-bis(methoxyethoxy)benzene in ether-based electrolytes. *Electrochimica Acta* **2017**, *246*, 251–258.

(29) Hu, J. J.; Long, G. K.; Liu, S.; Li, G. R.; Gao, X. P. A LiFSI-LiTFSI binary-salt electrolyte to achieve high capacity and cycle stability for a Li-S battery. *Chemical Communications* **2014**, *50*, 14647–14650.

(30) Park, M. S.; Ma, S. B.; Lee, D. J.; Im, D.; Doo, S. G.; Yamamoto, O. A highly reversible lithium metal anode. *Scientific Reports* **2014**, *4*, 1–8.

(31) Zhao-Karger, Z.; Zhao, X.; Fuhr, O.; Fichtner, M. Bisamide based non-nucleophilic electrolytes for rechargeable magnesium batteries. *RSC Advances* **2013**, *3*, 16330–16335.

(32) Danner, T.; Latz, A. On the influence of nucleation and growth of S8 and Li2S in lithium-sulfur batteries. *Electrochimica Acta* **2019**, *322*, 134719.

(33) Xu, Y.; Ye, Y.; Zhao, S.; Feng, J.; Li, J.; Chen, H.; Yang, A.; Shi, F.; Jia, L.; Wu, Y.; Yu, X.; Glans-Suzuki, P.-A.; Cui, Y.; Guo, J.; Zhang, Y. In Situ X-ray Absorption Spectroscopic Investigation of the Capacity Degradation Mechanism in Mg/S Batteries . *Nano Letters* **2019**, *19*, 2928–2934.

(34) Häcker, J.; Danner, C.; Sievert, B.; Biswas, I.; Zhao-Karger, Z.; Wagner, N.; Friedrich, K. A. Investigation of Magnesium–Sulfur Batteries using Electrochemical Impedance Spectroscopy. *Electrochimica Acta* **2020**, *338*, 135787.

(35) Aurbach, D.; Gofer, Y.; Schechter, A.; Chusid, O.; Gizbar, H.; Cohen, Y.; Moshkovich, M.; Turgeman, R. A comparison between the electrochemical behavior of reversible magnesium and lithium electrodes. *Journal of Power Sources* **2001**, *97-98*, 269 – 273, Proceedings of the 10th International Meeting on Lithium Batteries.

(36) Shterenberg, I.; Salama, M.; Gofer, Y.; Aurbach, D. Hexafluorophosphate-Based Solutions for Mg Batteries and the Importance of Chlorides. *Langmuir* **2017**, *33*, 9472–9478, PMID: 28651053.

(37) Sleightholme, A. E. S.; Vardar, G.; Chadwick, A. F.; Siegel, D. J.; DeWitt, S.; Thornton, K.; Monroe, C. W. Computational Model of Magnesium Deposition and Dissolution for Property Determination via Cyclic Voltammetry. *Journal of The Electrochemical Society* **2016**, *163*, A1813–A1821.

(38) Duman, S.; BaÇ§ci, S.; Tütüncü, H. M.; Srivastava, G. P. First-principles studies of ground-state and dynamical properties of MgS, MgSe, and MgTe in the rocksalt, zinc blende, wurtzite, and nickel arsenide phases. *Physical Review B - Condensed Matter and Materials Physics* **2006**, *73*, 1–14.

(39) Drews, J.; Danner, T.; Jankowski, P.; Vegge, T.; García Lastra, J. M.; Liu, R.; Zhao-Karger, Z.; Fichtner, M.; Latz, A. Modeling of Ion Agglomeration in Magnesium Electrolytes and its Impacts on Battery Performance. *ChemSusChem* **2020**, *13*, 3599–3604.

(40) Tonin, G.; Vaughan, G. B.; Bouchet, R.; Alloin, F.; Di Michiel, M.; Barchasz, C. Operando investigation of the lithium/sulfur battery system by coupled X-ray absorption tomography and X-ray diffraction computed tomography. *Journal of Power Sources* **2020**, *468*, 228287.

Graphical TOC Entry